

Learning to Act Robustly with View-Invariant Latent Actions

Youngjoon Jeong^{1*}, Junha Chun^{2*}, Taesup Kim^{1†}

¹Graduate School of Data Science, Seoul National University

²Department of Electrical and Computer Engineering, Seoul National University

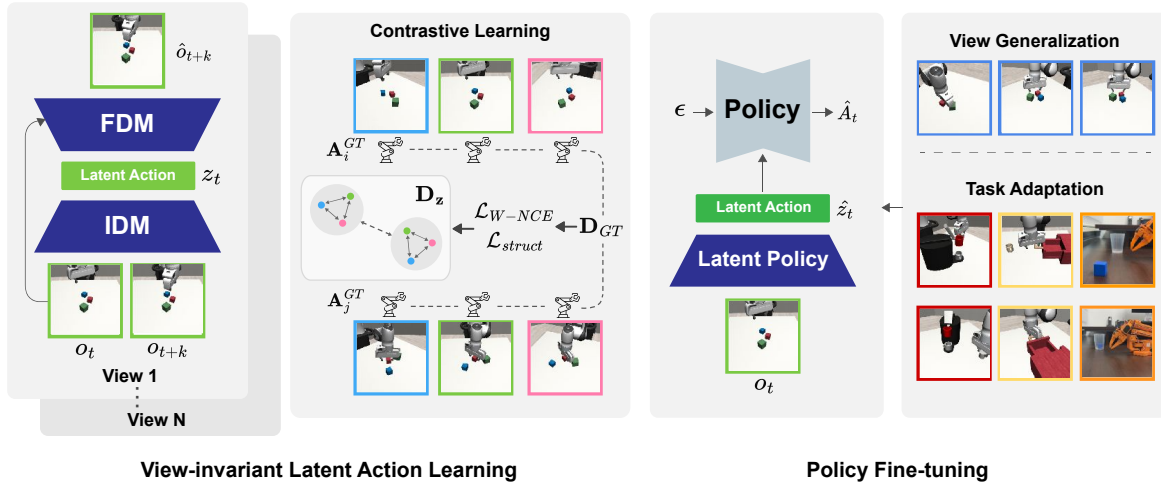


Figure 1. **VILA Overview.** Our method learns view-invariant latent actions by aligning them using action-aware contrastive learning along with predicting the future. A latent policy that predicts these latent actions from the current observation is then used as a vision encoder to condition a downstream visuomotor policy, yielding robust view generalization and task adaptation in simulation and the real-world.

Abstract

Vision-based robotic policies often struggle with even minor viewpoint changes, underscoring the need for view-invariant visual representations. This challenge becomes more pronounced in real-world settings, where viewpoint variability is unavoidable and can significantly disrupt policy performance. Existing methods typically learn invariance from multi-view observations at the scene level, but such approaches rely on visual appearance and fail to incorporate the physical dynamics essential for robust generalization. We propose View-Invariant Latent Action (VILA), which models a latent action capturing transition patterns across trajectories to learn view-invariant representations grounded in physical dynamics. VILA aligns these latent actions across viewpoints using an action-guided objective based on ground-truth action sequences. Experiments in both simulation and the real world show that VILA-based policies gener-

alize effectively to unseen viewpoints and transfer well to new tasks, establishing VILA as a strong pretraining framework that improves robustness and downstream learning performance. Demonstration videos can be found on our website: <https://joon-stack.github.io/VILA/>.

1. Introduction

Vision-based robotic policies are brittle to changes in camera viewpoint, posing a critical barrier to robust real-world deployment. While collecting large-scale, multi-view datasets is a straightforward way to expose policies to viewpoint variation, it incurs prohibitive data acquisition costs and scales poorly.

Prior approaches have largely focused on obtaining a scene-level visual representation that is stable under viewpoint changes. This is often achieved either by modifying observations (e.g., via novel view synthesis or geometric inputs) [7, 16, 34] or by pre-training encoders to learn invariant features [21, 27, 31]. Despite these different strategies,

*These authors contributed equally

†Corresponding author. Email: taesup.kim@snu.ac.kr

the underlying goal remains the same: enforcing robustness at the image-level. In practice, this means that a single compact feature vector is asked to summarize the entire image, including static layout and background, and at the same time carry all information about task-relevant motion. Enforcing viewpoint robustness at this level can therefore be unnecessarily demanding: it asks for invariance over a representation that is much broader than what is actually needed for control, and it does not explicitly distinguish between static context and the underlying dynamics that drive actions.

In this paper, we propose a different, more targeted approach. **Our key insight is that invariance should be enforced not on a static scene-level visual representation, but rather on the dynamics, the change in the scene that is relevant to the actions.** Representations of change are naturally more compact and predominantly capture how the agent and objects move, rather than how the entire scene looks from a particular viewpoint. To this end, we introduce **View-Invariant Latent Action (VILA)**, a novel pre-training framework described in Figure 1. VILA builds on the notion of latent actions [2, 26, 30, 37], which model dynamics as a compact code explaining the observed change between consecutive observations, but with a critical modification. VILA learns a latent action representation that encodes the change between observations. At the same time, we use ground-truth (GT) action sequences as *action-guided* alignment to shape this space with a weighted contrastive loss and a global similarity-alignment term, enforcing view-invariance directly in this dynamics-centered latent space.

2. Related Works

2.1. Viewpoint Robustness in Visuomotor Policies

A key challenge in visuomotor policy learning is generalizing to camera poses that differ between training and deployment. Prior work mainly tackles this via modifying the observations or learning view-robust representations.

The first family operates at the *observation level*. Multi-view calibrated datasets [13, 17, 20, 36] expose policies to multiple cameras, but typically with limited viewpoint diversity. Data augmentation methods instead synthesize or collect additional views so that the policy sees a wider range of poses; several recent approaches [7, 12, 34] use novel view synthesis (NVS) to expand labeled datasets. Other methods explicitly condition the policy on camera geometry, as in [16], which provides intrinsics, extrinsics, or per-pixel ray embeddings as additional inputs.

The second family operates at the *representation level* by learning view-robust visual encoders [21, 22, 27, 31, 33]. These methods train scene-level features to remain stable under camera motion while summarizing the entire image, which can conflate task-relevant motion with static context or visual appearances.

In contrast, VILA does not impose invariance on a scene-level representation. We enforce invariance only on the latent action, a compact representation of the system’s dynamics, so that model capacity is focused on how the agent and objects move rather than on full-scene appearance.

2.2. Latent Actions

Latent action models [2, 26, 30] learn compact dynamics representations by encoding the change between two observations o_t and o_{t+k} into a latent action z . This is typically done with an inverse dynamics model (IDM) inferring $z = \text{IDM}(o_t, o_{t+k})$ and a forward dynamics model (FDM) reconstructing $\hat{o}_{t+k} = \text{FDM}(o_t, z)$. To avoid trivial solutions, z is constrained by a low-dimensional bottleneck or vector quantization [30, 35, 37].

These dynamics representations have proved useful priors for world models [4, 14, 28] and policies [1, 2, 5, 8, 26, 30, 37]. However, existing work mainly optimizes latent actions to be predictive and useful for control, without explicitly targeting robustness to camera pose changes. Because latent actions are defined over changes between observations, they already emphasize motion rather than static appearance, which makes them a natural place to enforce additional viewpoint invariance. In VILA, we keep the standard latent action learning objective but add multi-view, action-guided regularization that forces latent actions for the same underlying motion to align across viewpoints, and then use this space as the interface for learning viewpoint-robust visuomotor policies.

3. Methods

Our proposed framework consists of two stages: (i) *latent action learning*, where we learn a compact, action-guided and view-invariant dynamics representation, and (ii) *latent behavior cloning*, where we train a latent policy that takes the current observation as input and predicts latent actions, so that this latent policy serves as a view-robust vision encoder that conditions a downstream visuomotor policy.

In the latent action learning stage, we pursue two primary objectives: (i) learning a base latent action representation that captures the underlying dynamics in a compact latent space; and (ii) enforcing view-invariance on this latent action using an action-aware contrastive objective. We build our base latent action learner on top of the LAOM framework [30], and then introduce our action-aware contrastive loss and structural regularizer. The resulting IDM is then reused in the latent behavior cloning stage, where we train a latent policy as an encoder.

3.1. Base Latent Action Learning

We first learn a base latent action representation following the core design of LAOM [30], which relies on a temporal consistency loss \mathcal{L}_{LA} in a compact latent space.

We index time by subscripts t and camera viewpoints by superscripts v , so o_t^v denotes the observation at time t from view v . A visual encoder E maps each observation o_t^v to a feature $s_t^v = E(o_t^v)$, and we sample a temporal offset $k \in \{1, \dots, K\}$ to obtain $s_{t+k}^v = E(o_{t+k}^v)$. The IDM infers a latent action $z_t^v = \text{IDM}(s_t^v, s_{t+k}^v)$, and the FDM predicts the future feature $\hat{s}_{t+k}^v = \text{FDM}(s_t^v, z_t^v)$.

The core temporal consistency loss \mathcal{L}_{LA} is defined as the mean squared error between this prediction \hat{s}_{t+k}^v and a stable target $s_{t+k}^{\text{tgt},v}$. The target is obtained by passing o_{t+k}^v through a separate, non-backpropagated encoder E^{tgt} , whose parameters are an EMA of the online encoder E . Let \mathcal{D}_k denote the set of all pairs (o_t^v, o_{t+k}^v) for which the segment $(t, t+k)$ exists in the dataset. Our latent action loss is

$$\mathcal{L}_{\text{LA}} = \mathbb{E}_{k \sim \mathcal{U}(1, K), (o_t^v, o_{t+k}^v) \sim \mathcal{D}_k} [\| \text{FDM}(s_t^v, z_t^v) - s_{t+k}^{\text{tgt},v} \|_2^2], \quad (1)$$

where $z_t^v = \text{IDM}(s_t^v, s_{t+k}^v)$. This loss encourages $(E, \text{IDM}, \text{FDM})$ to discover a compact latent action z_t^v that explains the change from o_t^v to o_{t+k}^v without reconstructing pixels. We use the same mini-batch construction described in Sec. 3.2 to obtain training samples for this objective.

3.2. Action-Guided Latent Action Invariance

To make the latent action invariant to camera viewpoint, we introduce an action-aware contrastive objective. The key idea is that latent actions inferred from different viewpoints should be close whenever their corresponding future GT action sequences are similar.

We construct each training batch as follows. We first sample a temporal offset $k \in \{1, \dots, K\}$ and then sample N base time indices $\{t_i\}_{i=1}^N$ such that the segment (t_i, t_i+k) and its GT action sequence $\mathbf{A}_i^{\text{GT}} = (a_{t_i}, \dots, a_{t_i+k-1})$ are available. For each base index t_i , we sample V random camera viewpoints and retrieve the corresponding observation pairs $\{(o_{t_i}^v, o_{t_i+k}^v)\}_{v=1}^V$, yielding $B = NV$ latent action samples per batch. We index these B transitions by a single index $i \in \{1, \dots, B\}$, so each i implicitly corresponds to a particular (t, v) pair, and denote the associated latent action by z_i and GT action sequence by \mathbf{A}_i^{GT} . Within each batch, k is held fixed so that all samples share the same prediction horizon.

We use the GT action sequences as supervision. For each sample i , let $\mathbf{A}_i^{\text{GT}} \in \mathbb{R}^{k \times D}$ denote the sequence of k actions. We first define a normalized squared distance between two sequences

$$d_{ij} = \frac{\| \mathbf{A}_i^{\text{GT}} - \mathbf{A}_j^{\text{GT}} \|_F^2}{kD}, \quad (2)$$

where $\| \cdot \|_F$ is the Frobenius norm. We then convert these distances into soft weights

$$w_{ij} = \frac{\exp(-d_{ij}/\beta)}{\sum_{\ell=1}^B \exp(-d_{i\ell}/\beta)}, \quad (3)$$

where $\beta > 0$ controls the sharpness of the distribution; larger w_{ij} indicate more similar action sequences.

Using these weights, we employ a weighted InfoNCE (supervised contrastive) loss [18, 19] that refines the *local* structure of the latent action space:

$$\mathcal{L}_{\text{W-NCE}} = - \sum_{i=1}^B \sum_{j=1, j \neq i}^B w_{ij} \log \frac{\exp(\text{sim}(z_i, z_j)/\tau)}{\sum_{\ell=1}^B \exp(\text{sim}(z_i, z_\ell)/\tau)}, \quad (4)$$

where $\text{sim}(z_i, z_j) = \frac{z_i^\top z_j}{\|z_i\| \|z_j\|}$ is cosine similarity and $\tau > 0$ is a temperature.

To capture the *global* structure, we introduce an auxiliary structural loss based on pairwise similarities. We treat each GT action sequence $\mathbf{A}_i^{\text{GT}} \in \mathbb{R}^{k \times D}$ as a single vector in \mathbb{R}^{kD} by flattening it (we reuse the same notation for brevity). We then L2-normalize latent actions and GT action vectors, $\hat{z}_i = z_i / \|z_i\|_2$ and $\hat{\mathbf{A}}_i^{\text{GT}} = \mathbf{A}_i^{\text{GT}} / \|\mathbf{A}_i^{\text{GT}}\|_2$, and form cosine-similarity matrices $S_z = \hat{Z} \hat{Z}^\top$ and $S_{\text{GT}} = \hat{A} \hat{A}^\top$, where the i -th rows of \hat{Z} and \hat{A} are \hat{z}_i^\top and $(\hat{\mathbf{A}}_i^{\text{GT}})^\top$, respectively. We then align these global similarity structures via

$$\mathcal{L}_{\text{struct}} = \| S_{\text{GT}} - S_z \|_F^2. \quad (5)$$

The total VILA representation loss is

$$\mathcal{L}_{\text{VILA}} = \mathcal{L}_{\text{LA}} + \lambda_1 \mathcal{L}_{\text{W-NCE}} + \lambda_2 \mathcal{L}_{\text{struct}}, \quad (6)$$

where λ_1 and λ_2 are weighting hyperparameters.

3.3. Latent Behavior Cloning

The latent behavior cloning stage learns a policy that predicts latent actions from the current observation so that no future frames are needed at test time. We train a latent policy π_z via behavior cloning:

$$\mathcal{L}_{\text{BC}} = \| \pi_z(s_t^v) - \text{IDM}(s_t^v, s_{t+k}^v) \|_2^2. \quad (7)$$

Since π_z operates in the pre-trained latent action space, it inherits its view-invariant, structured properties. During fine-tuning, π_z predicts latent actions from the current observation, and these are used as conditions for a downstream policy that outputs low-level actions.

4. Experimental Results

4.1. Viewpoint Setups

To train and evaluate view-robust policies, we construct a multi-view datasets by augmenting existing datasets with additional camera viewpoints. In simulation, we use five RoboSuite-based tasks [38]: (a) **Lift**: simple block lifting and (b) **Square: Pick & Place** with precision tasks from RoboMimic [23], (c) **Stack Three**: multiple block stacking, (d) **Coffee**: inserting pod in the coffee machine and closing,

Table 1. **Unseen View Generalization in Fine-tuned and Frozen Settings (Simulation).** For each of the 25 views in Figure 4, we evaluate average success rates (%) over 20 episodes and report for 10 seen views, 15 unseen views, and their ratio denoted as Rel.

Model	Lift			Square			Stack Three			Coffee			Mug Cleanup		
	Seen	Unseen	Rel.	Seen	Unseen	Rel.	Seen	Unseen	Rel.	Seen	Unseen	Rel.	Seen	Unseen	Rel.
Fine-Tuned															
VILA (Ours)	99.50	94.70	95.18	69.00	19.80	28.70	69.00	53.65	77.75	63.00	12.65	20.08	56.75	27.85	49.07
Vanilla	97.00	77.00	79.38	57.00	8.70	15.26	64.00	23.70	37.03	63.00	0.35	0.56	55.50	9.70	17.48
CLASS	96.50	65.00	67.36	54.00	9.00	16.67	30.00	10.35	34.50	28.00	0.35	1.25	22.00	6.35	28.86
ReViWo	83.00	38.00	45.78	5.00	0.35	7.00	0.00	0.00	0.00	0.00	0.00	0.00	0.00	0.00	0.00
KYC	72.00	46.00	63.89	14.00	0.00	0.00	1.90	0.00	0.00	10.70	0.00	0.00	4.00	0.00	0.00
Frozen															
VILA (Ours)	72.00	60.70	84.31	34.50	10.35	30.00	15.50	6.65	42.90	29.50	4.00	13.56	33.50	15.00	44.78
Vanilla	76.00	47.30	62.24	14.00	0.35	2.50	0.50	0.00	0.00	6.50	0.00	0.00	5.00	0.00	0.00
CLASS	93.90	65.00	69.22	25.00	0.35	1.40	0.50	0.00	0.00	6.00	0.00	0.00	4.00	0.00	0.00
ReViWo	78.00	40.70	52.18	1.50	0.00	0.00	0.00	0.00	0.00	0.50	0.00	0.00	0.00	0.00	0.00

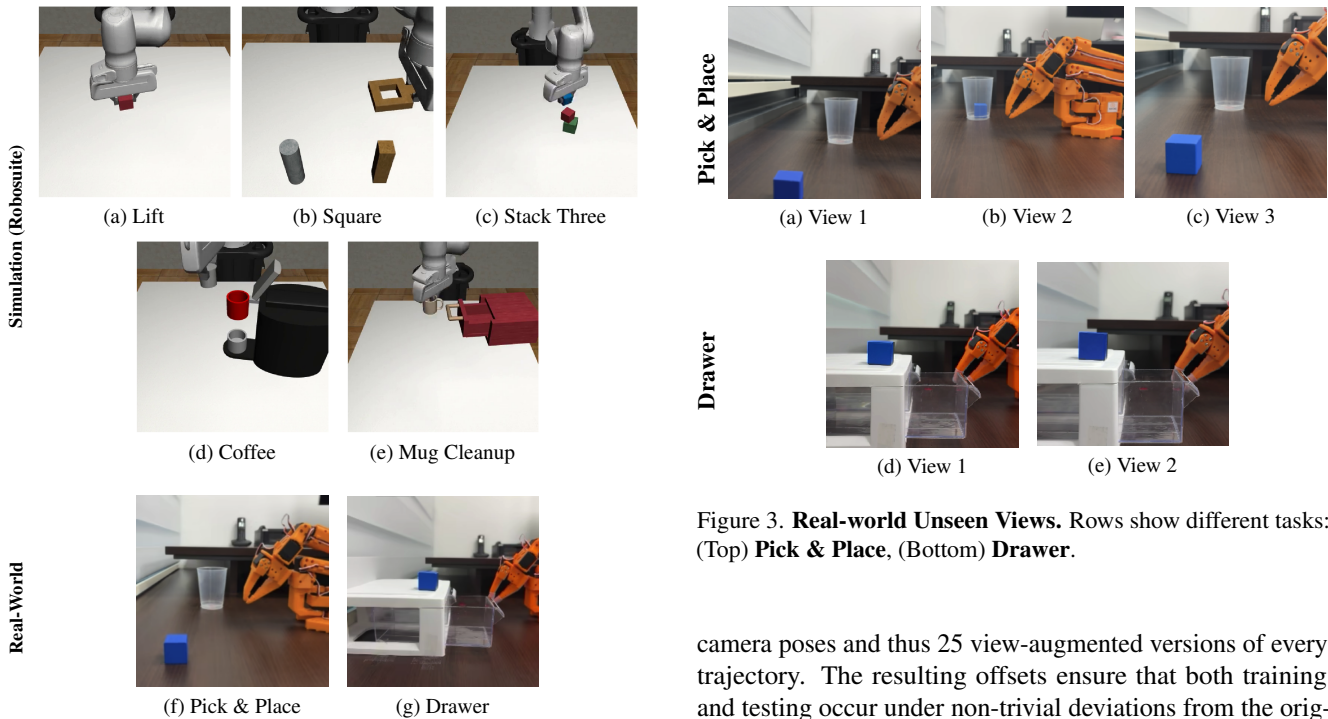


Figure 2. **Dataset Overview.** All images are displayed at the same scale. Top rows show simulation tasks, and the bottom row shows real-world experiments.

and (e) **Mug Cleanup**: opening the cabinet, placing mug in the cabinet, and closing tasks from MimicGen [24].

For each trajectory, we treat the original *agentview* as a reference and define a 5×5 grid over azimuth offsets in $[-90^\circ, +90^\circ]$ and elevation offsets in $[-15^\circ, +15^\circ]$, partitioning each range into five uniform bins.

We then sample one azimuth/elevation pair per grid cell as a relative offset from *agentview*, yielding 25 distinct

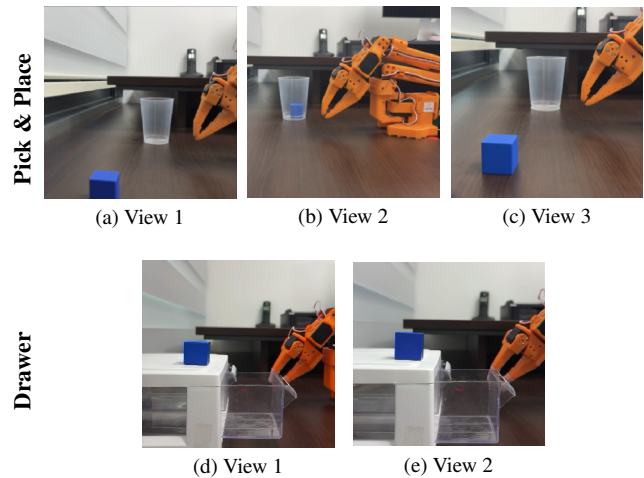


Figure 3. **Real-world Unseen Views.** Rows show different tasks: (Top) **Pick & Place**, (Bottom) **Drawer**.

camera poses and thus 25 view-augmented versions of every trajectory. The resulting offsets ensure that both training and testing occur under non-trivial deviations from the original camera. From these 25 views, we fix 10 for training encoders and policies and reserve the remaining 15 for evaluation (Figure 4). We also evaluate *extrapolated* viewpoints by choosing a base pose whose azimuth and elevation lie outside this sampling range and then perturbing it by $\pm 2^\circ$ along both axes, giving 8 additional test views. Exact azimuth and elevation values for all views are provided in the Appendix. Compared to prior multi-view setups used by our baselines [16, 21, 27], our benchmark covers a wide range of azimuth and elevation with fewer training views, leading to sparser camera coverage and a more challenging viewpoint generalization setting.

For real-world experiments, we use a self-collected single-view dataset of the SO-ARM101 robot [6] of two

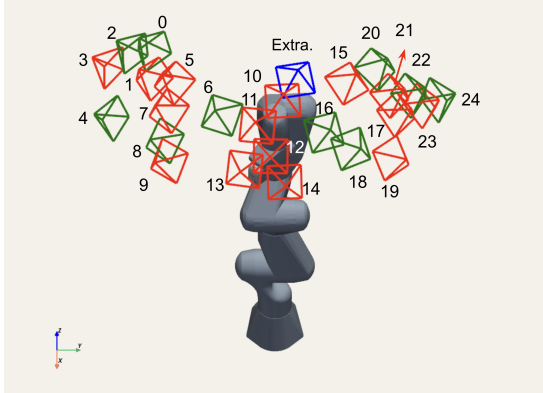


Figure 4. **Multi-View Camera Poses for Training and Evaluations.** Green poses are used for training the encoder and policy (seen), and red poses are reserved for evaluation (unseen). An extrapolated viewpoint (beyond 5×5 grid) is generated starting from the blue pose.

tasks: (f) **Pick & Place**: picking a block and placing inside the cup, and (g) **Drawer**: putting a block in the drawer and closing it. Since capturing identical trajectories from many physical cameras is challenging, we follow prior work [7, 34] and apply ZeroNVS [29] to augment the original videos with additional viewpoints. We vary the camera azimuth in $\{-5^\circ, 0^\circ, +5^\circ\}$, the vertical translation in $\{-5\text{cm}, 0\text{cm}, +5\text{cm}\}$, and the optical-axis translation in $\{-5\text{cm}, 0\text{cm}, +5\text{cm}\}$, producing 27 views including the original. We select 4 views for training and evaluate on 3 held-out views in Figure 3 that are disjoint from the training set.

4.2. Unseen View Generalization

Evaluation protocol. For each dataset and task, we first train an encoder and a visuomotor policy, and then evaluate generalization performance on seen and unseen viewpoints within the same task. We use an image resolution of 64×64 and a latent dimension of 128 for simulation tasks, whereas for real-world experiments, we use a resolution of 128×128 and a latent dimension of 512. All encoders are trained using the multi-view setup described in Sec. 4.1. For downstream control, we train a Diffusion Policy [9] with identical hyperparameters across all baselines, and measure its success rate separately for each viewpoint. Success rates are computed over multiple rollouts per view; additional details are reported in the Appendix.

We evaluate each representation in two downstream settings: (i) a *frozen* setting, where the encoder is fixed and only the policy parameters are trained, and (ii) a *fine-tuned* setting, where the encoder is updated jointly with the policy. The frozen setting highlights the inherent viewpoint generalization of the learned representation itself, while the fine-tuned setting measures its effectiveness as a strong initialization

Table 2. **View Generalization in Extrapolated Views in the Fine-tuned Setting.** Success rates (%) of fine-tuned policies on four simulation task evaluated under extrapolated camera poses (8 views). For each task, we evaluate success over 20 episodes per view, reporting the average success rate across these views. Note that the Coffee task is excluded because all methods failed under these extrapolated viewpoints.

Model	Lift	Square	Stack Three	Mug Cleanup
VILA (Ours)	93.10	3.10	35.00	11.85
Vanilla	28.10	0.60	6.25	2.50
CLASS	51.30	0.60	2.50	0.60
ReViWo	8.80	0.00	0.00	0.00
KYC	21.20	0.00	0.00	0.00

for task-specific policy learning.

Baselines. All baselines share the same downstream policy, observation preprocessing, and training schedule; only the encoder pre-training strategy and the presence of camera-conditioning (Know Your Camera [16] only) differ. This setup allows us to isolate the impact of the learned representation on unseen-view generalization.

- **Vanilla:** ImageNet-pretrained ResNet-18 encoder [11, 15] used directly for policy learning.
- **CLASS [21]:** Scene-level encoder trained with a weighted InfoNCE loss based on GT action-sequence distances.
- **ReViWo [27]:** View-invariant scene representation learned via decomposition of multi-view observations.
- **Know Your Camera (KYC) [16]:** Policy conditioned explicitly on camera parameters to aid cross-view generalization.

Table 3. **Real-World View Generalization.** Success rates (%) on real-world tasks. We evaluate **Pick & Place** on three unseen views and **Drawer** on two unseen views. Each setting consists of 10 episodes.

Model	Pick & Place				Drawer		
	View 1	View 2	View 3	Avg.	View 1	View 2	Avg.
VILA (Ours)	70.00	80.00	40.00	63.33	80.00	90.00	85.00
Vanilla	0.00	0.00	10.00	3.33	0.00	0.00	0.00
CLASS	10.00	30.00	0.00	13.33	0.00	0.00	0.00

Simulation results. Table 1 reports seen/unseen success rates and unseen/seen performance ratios (Rel.) across five simulated tasks in both *frozen* and *fine-tuned* settings. With fine-tuning, VILA attains the best unseen-view success on all tasks, including the harder tasks, while in the frozen setting it is the only method that maintains non-trivial performance on tasks where other approaches often collapse to near-zero under unseen views. Figure 5 further breaks down unseen-view

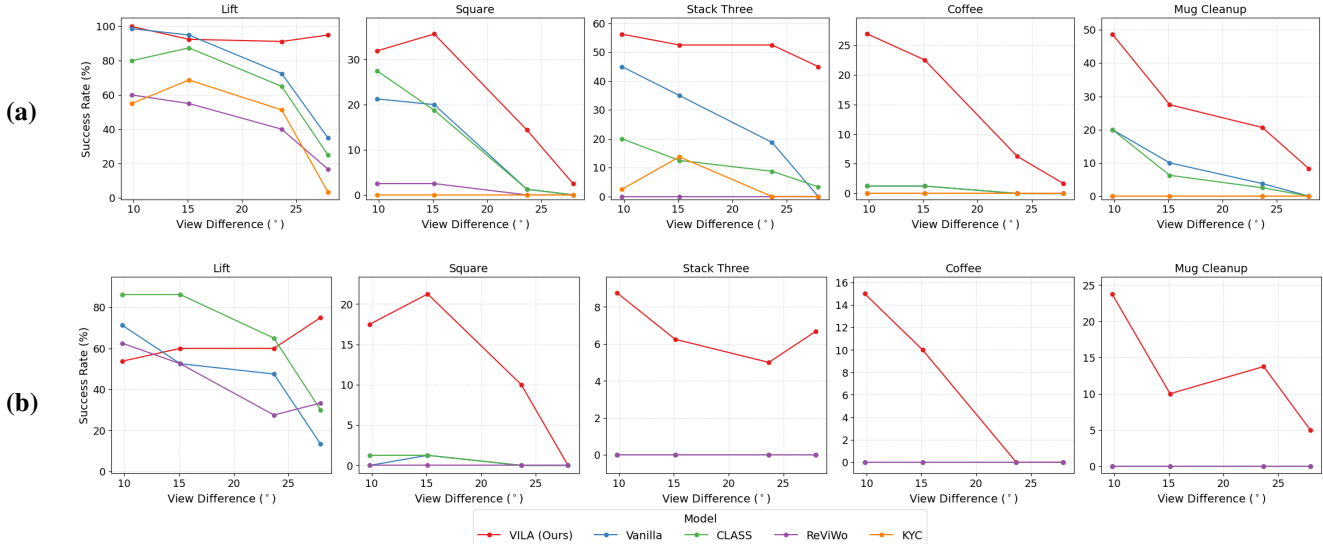


Figure 5. **Unseen View Generalization vs. Viewpoint Difference.** Success rates (%) (averaged over 20 episodes per each view) of VILA and baseline methods for view generalization under (a) *fine-tuned* and (b) *frozen* encoder settings. The success rates are shown with respect to angular differences from the training viewpoints. We evaluate 15 unseen camera viewpoints and, for each unseen view, compute its view difference to the closest training view among the 10 seen cameras, measured as the Euclidean norm in the (azimuth, elevation) space. Based on this, the 15 unseen views are sorted and partitioned into four groups (of sizes 4, 4, 4, and 3). On the x-axis, we plot the average nearest-view difference within each group, and on the y-axis we report the corresponding average success rate for that group.

performance as a function of viewpoint difference from seen views: across both settings, VILA consistently outperforms all baselines and its success degrades much more slowly as the gap from the nearest training camera increases. Table 2 shows that these gaps widen under extrapolated camera poses, with VILA retaining meaningful success rates while baselines largely fail.

Real-world results. Table 3 presents the performance on real-world **Pick & Place** and **Drawer** tasks under novel viewpoints. VILA achieves average success rates of 63.3% and 85.0%, respectively. In comparison, baseline methods show significantly lower performance, averaging below 13.3% on **Pick & Place** and recording 0% on the **Drawer** task. These results indicate that VILA offers improved robustness to viewpoint changes compared to the baselines.

4.3. Unseen Task Adaptation

Evaluation protocol. To investigate whether representations learned on one dataset provide useful priors for other tasks, we transfer encoders trained on the Stack Three task to a new Coffee task under a single-view setup (i.e., policy is trained and evaluated on the single identical view). Concretely, we take each encoder pre-trained on Stack Three in the multi-view setting (Sec. 4.1) and use it to initialize a visuomotor policy on Coffee, then fine-tune the encoder and policy jointly using only a small subset of the Coffee demonstrations. Note that policies for Coffee task are trained with

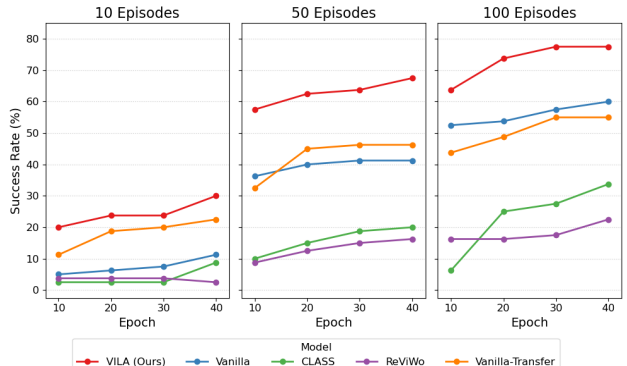


Figure 6. **Unseen Task Adaptation.** Success rates (%) of VILA and baseline methods when adapting from Stack Three to Coffee. For each data point, we report the average success over 40 episodes using the training view only, plotted as a function of the number of labeled trajectories and training epochs.

1,000 episodes in Section 4.2. For each encoder, we train single-view policies from two different camera viewpoints and report performance as the average success rate across these views. This setup allows us to assess both cross-task transfer and whether each encoder provides a viewpoint-generalized prior that carries over to a new task.

Baselines. The Vanilla baseline denotes training a policy directly on the Coffee task in the single-view setting, using only the chosen Coffee subset and an ImageNet-pretrained ResNet encoder, without any multi-view or cross-task pre-training. The Vanilla-Transfer baseline instead first fine-tunes the Vanilla encoder on the Stack Three multi-view task (as in our unseen-view generalization experiments), and then uses this fine-tuned encoder as initialization for subsequent single-view training on Coffee. All other methods follow the same protocol: we start from their respective encoders pre-trained on the Stack Three multi-view dataset and then fine-tune them on the single-view Coffee task.

Results. Figure 6 summarizes unseen task adaptation on Coffee under different labeled data budgets. Across all budgets, VILA provides a stronger prior than the Vanilla baseline, while other encoders often match or even underperform Vanilla trained from scratch. Thus, not all multi-view pre-training is helpful for cross-task adaptation: enforcing scene-level invariance can produce less transferable priors that might overfit to task-specific appearances, whereas VILA’s latent-action representation yields a viewpoint-generalized and dynamics-centered prior that remains useful even with limited Coffee data.

5. Discussion

5.1. Ablation Studies

We conduct a comprehensive ablation study to validate the key design choices of VILA. Unless otherwise noted, all ablations are performed on the Lift task in the fine-tuned setting, and we report success rates on unseen views. Our default configuration uses an action-guided Weighted InfoNCE loss combined with a structural distance-alignment loss, L2 distance between action sequences for weight and cosine similarity for structural alignment, a latent action dimension of 128, and a random offset sampling range of 10 steps (Sec. 3.2). The results are summarized in Table 4.

Loss function. Removing the action-based weighting with standard InfoNCE or omitting the structural loss both degrade unseen-view success compared to the full objective, indicating that the two components are complementary. Using the base latent-action loss alone performs even worse, confirming that neither the structural loss nor the action-based weighting is helpful. Alternative global regularizers based on distance-matrix or CKA-style alignment also underperform our distance-based structural loss. Adding an auxiliary action-regression head further harms unseen-view performance, suggesting that actions are more effective as soft similarity supervision than as direct regression targets.

Table 4. **Ablation study of VILA components.** Seen and Unseen denote success rates (%) averaged over 20 episodes across the 10 training views and 15 held-out views on the Lift task in the fine-tuned setting.

Method	Seen	Unseen	Rel.
VILA (Ours)	99.50	94.70	95.18
<i>Loss function (default: \mathcal{L}_{LA} & \mathcal{L}_{W-NCE} & \mathcal{L}_{struct})</i>			
\mathcal{L}_{LA} & \mathcal{L}_{W-NCE} & \mathcal{L}_{CKA}	98.50	92.00	93.40
\mathcal{L}_{LA} & \mathcal{L}_{W-NCE}	99.00	91.70	92.63
\mathcal{L}_{LA} & \mathcal{L}_{NCE}	95.50	90.00	94.24
\mathcal{L}_{LA} & \mathcal{L}_{struct}	99.50	84.30	84.72
\mathcal{L}_{LA}	93.00	79.50	85.48
\mathcal{L}_{LA} & \mathcal{L}_{W-NCE} & \mathcal{L}_{struct} & \mathcal{L}_{act}	98.00	86.70	88.47
<i>Action-sequence distance</i>			
Dynamic Time Warping (DTW)	96.40	89.20	92.53
<i>Offset sampling strategy (default: random offset 1–10)</i>			
Random offset 1–16	99.50	93.70	94.17
Random offset 1–5	98.50	92.30	93.71
Fixed offset 10	97.50	90.00	92.31
<i>Latent action dimension (default: 128)</i>			
32 dimensions	98.00	88.00	89.80
64 dimensions	97.00	84.70	87.32
256 dimensions	98.00	88.70	90.51
512 dimensions	96.00	90.00	93.75
Loss term definitions. \mathcal{L}_{NCE} : standard InfoNCE with positives from the same transition and negatives from others; \mathcal{L}_{CKA} : RBF-kernel CKA-based structural alignment of latent actions and GT-actions; \mathcal{L}_{act} : auxiliary action-prediction loss.			

Offset sampling strategy. Sampling temporal offsets uniformly from $\{1, \dots, 10\}$ when constructing action sequences yields the best unseen-view generalization. Smaller or larger maximum offsets, or a fixed offset, consistently degrade performance, suggesting that a moderate offset range captures dynamics most effectively.

Distance metric. Replacing our L2 distance in weighted contrastive learning and cosine similarity in structural alignment with Dynamic Time Warping (DTW) [3] lowers unseen-view success. Unlike prior work that applies DTW to longer trajectories (e.g., 16 steps in CLASS [21]), our sequences of up to 10 steps already work well with L2. Since we resample sequence lengths (1–10) at every batch, precomputing exact DTW distances is impractical, so we instead use Soft-DTW [10], whose approximation error and higher computational cost do not translate into better performance in our setting.

Latent action dimension. A latent dimension 128 gives the best unseen-view generalization. Both smaller and much larger latent spaces hurt performance, suggesting that 128

offers a good trade-off between expressivity and regularization.

5.2. Representation Quality Analysis

We evaluate the quality of the representation using entropy-based metrics that capture the viewpoint invariance and dynamics-aware semantics. For each encoder, we sample 12,500 transitions (500 per view) from the multi-view dataset, extract features before and after policy fine-tuning, and for each feature compute its $k = 50$ nearest neighbors (L2) and the corresponding entropies.

Table 5. **View and Action Entropy.** Entropy-based analysis of representation quality before and after policy fine-tuning in Lift dataset. “Seen” and “Unseen” denote view entropies (higher is better, \uparrow) computed over the 25 views, respectively, while “Action” denotes action entropy (lower is better, \downarrow) based on 10 clustered action classes. The upper-bound row corresponds to the entropy of a uniform distribution over 25 views (Seen/Unseen) and 10 action clusters (Action).

Model	Seen (\uparrow)	Unseen (\uparrow)	Action (\downarrow)
Upper Bound	3.219	3.219	2.303
Before Fine-tuning			
VILA (Ours)	2.757	2.495	0.934
CLASS	2.641	2.159	1.041
ReViWo	2.479	1.83	1.132
Fine-Tuned			
VILA (Ours)	2.803	2.548	0.829
Vanilla	2.707	2.121	1.445
CLASS	2.624	1.933	1.006
ReViWo	2.597	2.244	1.177
KYC	2.149	1.793	1.254

View entropy. View entropy measures how mixed camera views are in each feature’s local neighborhood. For each feature, we take the distribution of view IDs among its k nearest neighbors, compute the Shannon entropy [32] of this categorical distribution, and average over all features. *Higher* view entropy means neighbors are drawn more uniformly from the 25 views, indicating a more view-invariant representation.

Action entropy. To check that invariance does not harm dynamics-aware semantics, we define an action entropy that measures how consistently features group similar future dynamics. We cluster all 10-step GT action sequences $\{a_t, \dots, a_{t+9}\}$ into $K = 10$ action classes using k -means and assign each observation o_t the label c_t of its associated sequence. For each feature, we look at the class labels of its k nearest neighbors, compute the entropy over this distribution, and average across features. Here, *lower* action

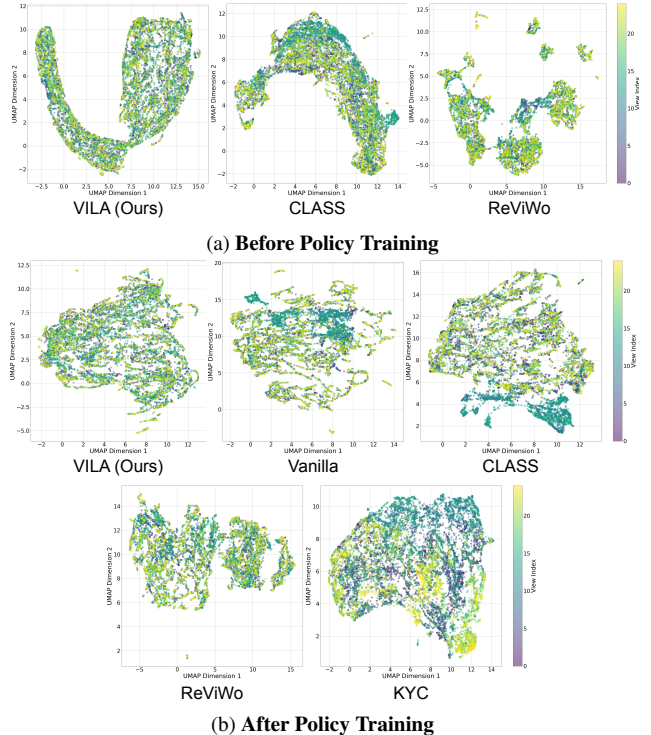


Figure 7. **UMAP of encoder representations across 25 views.** On Lift, baselines show distinct clusters for unseen views (especially for views 10–14), whereas VILA representations are more uniformly mixed across views, indicating stronger view invariance both before and after policy training.

entropy is better, indicating that visual features tend to cluster according to similar action outcomes.

Results. Table 5 reports view and action entropy on the Lift dataset (other tasks are in the Appendix). VILA achieves the *highest view entropy* on both seen and unseen views, indicating a strongly view-invariant representation, while also obtaining the *lowest action entropy*. This shows that enforcing invariance on *dynamics* rather than entire scenes lets VILA simultaneously achieve strong viewpoint mixing and tight clusters of features with similar action outcomes.

UMAP plots. We visualize the learned representations with UMAP [25]. Figures 7a and 7b show 2D embeddings colored by view index. For baselines, unseen views (especially Views 10–14) form separate clusters, whereas VILA intermingles them with seen views. This pattern matches our entropy analysis that VILA has the highest view entropy. Additional UMAP plots for latent actions and other datasets are in the Appendix.

6. Conclusion

We tackle viewpoint robustness in visuomotor control with VILA, a pre-training framework that enforces invariance on latent action instead of scene-level visual features. Building on latent action models with an action-guided contrastive loss and structure alignment, VILA learns a latent space that is both view-invariant and aligned with control dynamics, leading to consistent gains in unseen-view generalization and data-efficient unseen task adaptation across five simulated tasks and a real-world SO-ARM setup. These suggest that targeting invariance at the level of dynamics is a promising direction for robust visuomotor policies under camera changes.

Limitations. Our experiments assume access to multi-view observations of a given task, which are straightforward to generate in simulation but more involved to collect in real-world setups. In the real-robot setting, we follow prior work and use ZeroNVS to obtain additional viewpoints, so part of the observed robustness may reflect the behavior of the underlying NVS model. Finally, we primarily study robustness to camera pose; extending the same action-guided invariance principle to other sources of variation (e.g., lighting, backgrounds, object appearance) is a natural next step toward more broadly robust visuomotor policies.

References

- [1] AgiBot-World-Contributors, Qingwen Bu, Jisong Cai, Li Chen, Xiuqi Cui, Yan Ding, Siyuan Feng, Shenyuan Gao, Xindong He, Xuan Hu, Xu Huang, Shu Jiang, Yuxin Jiang, Cheng Jing, Hongyang Li, Jialu Li, Chiming Liu, Yi Liu, Yuxiang Lu, Jianlan Luo, Ping Luo, Yao Mu, Yuehan Niu, Yixuan Pan, Jiangmiao Pang, Yu Qiao, Guanghui Ren, Cheng Ruan, Jiaqi Shan, Yongjian Shen, Chengshi Shi, Mingkan Shi, Modi Shi, Chonghao Sima, Jianheng Song, Huijie Wang, Wenhao Wang, Dafeng Wei, Chengen Xie, Guo Xu, Junchi Yan, Cunbiao Yang, Lei Yang, Shukai Yang, Maoqing Yao, Jia Zeng, Chi Zhang, Qinglin Zhang, Bin Zhao, Chengyue Zhao, Jiaqi Zhao, and Jianchao Zhu. Agibot world colosse: A large-scale manipulation platform for scalable and intelligent embodied systems, 2025. 2
- [2] Erik Bauer, Elvis Nava, and Robert K. Katzschmann. Latent action diffusion for cross-embodiment manipulation, 2025. 2
- [3] Donald J. Berndt and James Clifford. Using dynamic time warping to find patterns in time series. In *Proceedings of the 3rd International Conference on Knowledge Discovery and Data Mining*, page 359–370. AAAI Press, 1994. 7
- [4] Jake Bruce, Michael Dennis, Ashley Edwards, Jack Parker-Holder, Yuge Shi, Edward Hughes, Matthew Lai, Aditi Mavalankar, Richie Steigerwald, Chris Apps, Yusuf Aytar, Sarah Bechtle, Feryal Behbahani, Stephanie Chan, Nicolas Heess, Lucy Gonzalez, Simon Osindero, Sherjil Ozair, Scott Reed, Jingwei Zhang, Konrad Zolna, Jeff Clune, Nando de Freitas, Satinder Singh, and Tim Rocktäschel. Genie: Generative interactive environments, 2024. 2
- [5] Qingwen Bu, Yanting Yang, Jisong Cai, Shenyuan Gao, Guanghui Ren, Maoqing Yao, Ping Luo, and Hongyang Li. Univla: Learning to act anywhere with task-centric latent actions. *arXiv preprint arXiv:2505.06111*, 2025. 2
- [6] Remi Cadene, Simon Alibert, Alexander Soare, Quentin Gallouedec, Adil Zouitine, Steven Palma, Pepijn Kooijmans, Michel Aractingi, Mustafa Shukor, Dana Aubakirova, Martino Russi, Francesco Capuano, Caroline Pascal, Jade Choghari, Jess Moss, and Thomas Wolf. Lerobot: State-of-the-art machine learning for real-world robotics in pytorch. <https://github.com/huggingface/lerobot>, 2024. 4
- [7] Lawrence Yunliang Chen, Chenfeng Xu, Karthik Dharmarajan, Muhammad Zubair Irshad, Richard Cheng, Kurt Keutzer, Masayoshi Tomizuka, Quan Vuong, and Ken Goldberg. Rovi-aug: Robot and viewpoint augmentation for cross-embodiment robot learning, 2024. 1, 2, 5
- [8] Xiaoyu Chen, Hangxing Wei, Pushi Zhang, Chuheng Zhang, Kaixin Wang, Yanjiang Guo, Rushuai Yang, Yucen Wang, Xinquan Xiao, Li Zhao, Jianyu Chen, and Jiang Bian. villa-x: Enhancing latent action modeling in vision-language-action models, 2025. 2
- [9] Cheng Chi, Siyuan Feng, Yilun Du, Zhenjia Xu, Eric Cousineau, Benjamin Burchfiel, and Shuran Song. Diffusion policy: Visuomotor policy learning via action diffusion. In *Proceedings of Robotics: Science and Systems (RSS)*, 2023. 5
- [10] Marco Cuturi and Mathieu Blondel. Soft-dtw: a differentiable loss function for time-series, 2018. 7
- [11] Jia Deng, Wei Dong, Richard Socher, Li-Jia Li, Kai Li, and Li Fei-Fei. Imagenet: A large-scale hierarchical image database. In *2009 IEEE Conference on Computer Vision and Pattern Recognition*, pages 248–255, 2009. 5
- [12] Haoran Ding, Anqing Duan, Zezhou Sun, Dezhen Song, and Yoshihiko Nakamura. Imagination at inference: Synthesizing in-hand views for robust visuomotor policy inference. *arXiv preprint arXiv:2509.15717*, 2025. 2
- [13] Hao-Shu Fang, Hongjie Fang, Zhenyu Tang, Jirong Liu, Chenxi Wang, Junbo Wang, Haoyi Zhu, and Cewu Lu. Rh20t: A comprehensive robotic dataset for learning diverse skills in one-shot. In *2024 IEEE International Conference on Robotics and Automation (ICRA)*, pages 653–660. IEEE, 2024. 2
- [14] Shenyuan Gao, Siyuan Zhou, Yilun Du, Jun Zhang, and Chuang Gan. Adaworld: Learning adaptable world models with latent actions. In *International Conference on Machine Learning (ICML)*, 2025. 2
- [15] Kaiming He, Xiangyu Zhang, Shaoqing Ren, and Jian Sun. Deep residual learning for image recognition, 2015. 5
- [16] Tianchong Jiang, Jingtian Ji, Xiangshan Tan, Jiading Fang, Anand Bhattad, Vitor Guizilini, and Matthew R. Walter. Do you know where your camera is? view-invariant policy learning with camera conditioning, 2025. 1, 2, 4, 5
- [17] Alexander Khazatsky, Karl Pertsch, Suraj Nair, Ashwin Balakrishna, Sudeep Dasari, Siddharth Karamcheti, Soroush Nasiriany, Mohan Kumar Srirama, Lawrence Yunliang Chen,

- Kirsty Ellis, Peter David Fagan, Joey Hejna, Masha Itkina, Marion Lepert, Yecheng Jason Ma, Patrick Tree Miller, Jimmy Wu, Suneel Belkhale, Shivin Dass, Huy Ha, Arhan Jain, Abraham Lee, Youngwoon Lee, Marius Memmel, Sungjae Park, Ilija Radosavovic, Kaiyuan Wang, Albert Zhan, Kevin Black, Cheng Chi, Kyle Beltran Hatch, Shan Lin, Jingpei Lu, Jean Mercat, Abdul Rehman, Pannag R Sanketi, Archit Sharma, Cody Simpson, Quan Vuong, Homer Rich Walke, Blake Wulfe, Ted Xiao, Jonathan Heewon Yang, Arefeh Yavary, Tony Z. Zhao, Christopher Agia, Rohan Bajjal, Mateo Guaman Castro, Daphne Chen, Qiuyu Chen, Trinity Chung, Jaimyn Drake, Ethan Paul Foster, Jensen Gao, David Antonio Herrera, Minh Heo, Kyle Hsu, Jiaheng Hu, Donovan Jackson, Charlotte Le, Yunshuang Li, Roy Lin, Zehan Ma, Abhiram Maddukuri, Suvir Mirchandani, Daniel Morton, Tony Nguyen, Abigail O'Neill, Rosario Scalise, Derrick Seale, Victor Son, Stephen Tian, Emi Tran, Andrew E. Wang, Yilin Wu, Annie Xie, Jingyun Yang, Patrick Yin, Yunchu Zhang, Osbert Bastani, Glen Berseth, Jeannette Bohg, Ken Goldberg, Abhinav Gupta, Abhishek Gupta, Dinesh Jayaraman, Joseph J Lim, Jitendra Malik, Roberto Martín-Martín, Subramanian Ramamoorthy, Dorsa Sadigh, Shuran Song, Jiajun Wu, Michael C. Yip, Yuke Zhu, Thomas Kollar, Sergey Levine, and Chelsea Finn. DROID: A Large-Scale In-The-Wild Robot Manipulation Dataset. In *Proceedings of Robotics: Science and Systems*, Delft, Netherlands, 2024. 2
- [18] Prannay Khosla, Piotr Teterwak, Chen Wang, Aaron Sarna, Yonglong Tian, Phillip Isola, Aaron Maschinot, Ce Liu, and Dilip Krishnan. Supervised contrastive learning, 2021. 3
- [19] Taeyoung Kim, Jimin Lee, Myungkyu Koo, Dongyoung Kim, Kyungmin Lee, Changyeon Kim, Younggyo Seo, and Jinwoo Shin. Contrastive representation regularization for vision-language-action models, 2025. 3
- [20] Vikash Kumar, Rutav Shah, Gaoyue Zhou, Vincent Moens, Vittorio Caggiano, Abhishek Gupta, and Aravind Rajeswaran. Robohive: A unified framework for robot learning. *Advances in Neural Information Processing Systems*, 36:44323–44340, 2023. 2
- [21] Sung-Wook Lee, Xuhui Kang, Brandon Yang, and Yen-Ling Kuo. Class: Contrastive learning via action sequence supervision for robot manipulation. In *Conference on Robot Learning (CoRL)*, 2025. 1, 2, 4, 5, 7
- [22] Fanfan Liu, Feng Yan, Liming Zheng, Yiyang Huang, Chengjian Feng, and Lin Ma. Robouniview: Visual-language model with unified view representation for robotic manipulation. *arXiv preprint 2406.18977*, 2024. 2
- [23] Ajay Mandlekar, Danfei Xu, Josiah Wong, Soroush Nasiriany, Chen Wang, Rohun Kulkarni, Li Fei-Fei, Silvio Savarese, Yuke Zhu, and Roberto Martín-Martín. What matters in learning from offline human demonstrations for robot manipulation. In *arXiv preprint arXiv:2108.03298*, 2021. 3, 2
- [24] Ajay Mandlekar, Soroush Nasiriany, Bowen Wen, Iretiayo Akinola, Yashraj Narang, Linxi Fan, Yuke Zhu, and Dieter Fox. Mimicgen: A data generation system for scalable robot learning using human demonstrations. In *7th Annual Conference on Robot Learning*, 2023. 4
- [25] Leland McInnes, John Healy, and James Melville. Umap: Uniform manifold approximation and projection for dimension reduction, 2020. 8
- [26] Alexander Nikulin, Ilya Zisman, Denis Tarasov, Nikita Lyubaykin, Andrei Polubarov, Igor Kiselev, and Vladislav Kurenkov. Latent action learning requires supervision in the presence of distractors, 2025. 2
- [27] Jing-Cheng Pang, Nan Tang, kaiyuan Li, Yuting Tang, Xin-Qiang Cai, Zhen-Yu Zhang, Gang Niu, Sugiyama Masashi, and Yang Yu. Learning view-invariant world models for visual robotic manipulation. In *International Conference on Learning Representations (ICLR)*, 2025. 1, 2, 4, 5
- [28] Zhongwei Ren, Yunchao Wei, Xun Guo, Yao Zhao, Bingyi Kang, Jiashi Feng, and Xiaojie Jin. Videoworld: Exploring knowledge learning from unlabeled videos, 2025. 2
- [29] Kyle Sargent, Zizhang Li, Tanmay Shah, Charles Herrmann, Hong-Xing Yu, Yunzhi Zhang, Eric Ryan Chan, Dmitry Lagun, Li Fei-Fei, Deqing Sun, and Jiajun Wu. ZeroNVS: Zero-shot 360-degree view synthesis from a single real image. *arXiv preprint arXiv:2310.17994*, 2023. 5
- [30] Dominik Schmidt and Minqi Jiang. Learning to act without actions, 2024. 2
- [31] Younggyo Seo, Junsu Kim, Stephen James, Kimin Lee, Jinwoo Shin, and Pieter Abbeel. Multi-view masked world models for visual robotic manipulation, 2023. 1, 2
- [32] Claude Elwood Shannon. A mathematical theory of communication. *The Bell System Technical Journal*, 27:379–423, 1948. 8
- [33] Le Shi, Yifei Shi, Xin Xu, Tenglong Liu, Junhua Xi, and Chengyuan Chen. Nvspolicy: Adaptive novel-view synthesis for generalizable language-conditioned policy learning. *ArXiv*, abs/2505.10359, 2025. 2
- [34] Stephen Tian, Blake Wulfe, Kyle Sargent, Katherine Liu, Sergey Zakharov, Vitor Guizilini, and Jiajun Wu. View-invariant policy learning via zero-shot novel view synthesis, 2025. 1, 2, 5
- [35] Aaron van den Oord, Oriol Vinyals, and Koray Kavukcuoglu. Neural discrete representation learning, 2018. 2
- [36] Homer Walke, Kevin Black, Abraham Lee, Moo Jin Kim, Max Du, Chongyi Zheng, Tony Zhao, Philippe Hansen-Estruch, Quan Vuong, Andre He, Vivek Myers, Kuan Fang, Chelsea Finn, and Sergey Levine. Bridgedata v2: A dataset for robot learning at scale. In *Conference on Robot Learning (CoRL)*, 2023. 2
- [37] Seonghyeon Ye, Joel Jang, Byeongguk Jeon, Sejune Joo, Jianwei Yang, Baolin Peng, Ajay Mandlekar, Reuben Tan, Yu-Wei Chao, Bill Yuchen Lin, Lars Liden, Kimin Lee, Jianfeng Gao, Luke Zettlemoyer, Dieter Fox, and Minjoon Seo. Latent action pretraining from videos, 2025. 2
- [38] Yuke Zhu, Josiah Wong, Ajay Mandlekar, Roberto Martín-Martín, Abhishek Joshi, Soroush Nasiriany, Yifeng Zhu, and Kevin Lin. robosuite: A modular simulation framework and benchmark for robot learning. In *arXiv preprint arXiv:2009.12293*, 2020. 3

Learning to Act Robustly with View-Invariant Latent Actions

Supplementary Material

A. Implementation Details

We provide the implementation details used for view generation, NVS generation, VILA training, baselines and diffusion policy training.

A.1. View Configurations

For reproducibility, Tables 6 and 7 list the exact world-frame camera poses (positions and MuJoCo quaternions) for all views used in this paper.

A.2. ZeroNVS Configurations

We utilized the official open-source implementation of ZeroNVS¹ and the pretrained checkpoint to generate novel views in our real-world experiments using SO-ARM101. Configurations for this process is as Table 8. We created 26 more combinations of novel views of our dataset and selected 4 views of azimuth, vertical and optical axis translation of $(0.0^\circ, -5\text{cm}, 5\text{cm})$, $(5^\circ, 0\text{cm}, -5\text{cm})$, $(-5^\circ, 5\text{cm}, 0\text{cm})$ and the original data representing $(0.0^\circ, 0.0\text{cm}, 0.0\text{cm})$ to cover all variations of each axis.

A.3. VILA Configurations

We train VILA with a two-stage pipeline: (i) latent action pre-training from multi-view videos, and (ii) latent behavior cloning in the learned latent space. Unless otherwise specified, we use a single configuration across all datasets and tasks, summarized in Table 9.

A.4. Baseline Implementations

CLASS. We adapt CLASS from the official open-source implementation² to our setting by applying its contrastive objective on top of our Stage-1 encoder. To ensure a fair comparison, we match the configuration used in VILA: an image resolution of 64×64 and latent dimension of 128 for simulation, and 128×128 with a dimension of 512 for real-world experiments.

ReViWo. For ReViWo, we follow the official implementation³. We use input image sizes of 64×64 for simulation and 128×128 for real-world tasks. Since ReViWo is ViT-based, we adjust the token and hidden dimensions so that the final representation dimension matches 128 for simulation and 512 for the real-world setting, ensuring that all methods use the same latent dimensionality as VILA.

View	x	y	z	q_w	q_x	q_y	q_z
View 00	0.0981	-0.4091	1.4249	0.9451	0.3051	0.0361	0.1117
View 01	0.2021	-0.4080	1.3951	0.9159	0.3304	0.0773	0.2144
View 02	0.0473	-0.4811	1.3677	0.9293	0.3662	0.0180	0.0456
View 03	0.0204	-0.5587	1.2741	0.8937	0.4483	0.0082	0.0163
View 04	0.2175	-0.5482	1.2234	0.8577	0.4786	0.0915	0.1639
View 05	0.2523	-0.3380	1.4240	0.9029	0.2925	0.0971	0.2998
View 06	0.3973	-0.1771	1.4131	0.7947	0.2686	0.1743	0.5157
View 07	0.3278	-0.3572	1.3663	0.8665	0.3429	0.1335	0.3374
View 08	0.3985	-0.3722	1.2939	0.8271	0.3965	0.1722	0.3592
View 09	0.4504	-0.3576	1.2489	0.7957	0.4215	0.2036	0.3843
View 10	0.3738	0.0263	1.4587	0.6572	0.1817	0.1950	0.7051
View 11	0.4394	-0.0577	1.4061	0.7102	0.2465	0.2162	0.6230
View 12	0.5130	-0.0142	1.3349	0.6579	0.2846	0.2769	0.6400
View 13	0.5352	-0.1022	1.2945	0.6950	0.3327	0.2752	0.5749
View 14	0.5651	0.0328	1.2635	0.6105	0.3135	0.3322	0.6470
View 15	0.2890	0.2414	1.4574	0.4081	0.1136	0.2428	0.8727
View 16	0.4437	0.1645	1.3781	0.5336	0.2036	0.2926	0.7669
View 17	0.3112	0.4094	1.3336	0.2929	0.1271	0.3773	0.8693
View 18	0.4612	0.2553	1.3178	0.4627	0.2092	0.3549	0.7850
View 19	0.4271	0.3932	1.2399	0.3535	0.1908	0.4350	0.8059
View 20	0.2071	0.3366	1.4443	0.2611	0.0775	0.2737	0.9225
View 21	0.2687	0.3871	1.3800	0.2793	0.1059	0.3384	0.8923
View 22	0.2279	0.4535	1.3414	0.2124	0.0903	0.3806	0.8955
View 23	0.2285	0.4949	1.2941	0.1935	0.0927	0.4220	0.8808
View 24	0.1605	0.5482	1.2553	0.1258	0.0657	0.4585	0.8773

Table 6. **Exact Camera Poses for the 25 Main Views.** Positions are given in the world frame (MuJoCo’s default metric units, i.e., meters), and orientations are MuJoCo quaternions (q_w, q_x, q_y, q_z) .

View	x	y	z	q_w	q_x	q_y	q_z
Extra View 00	0.2902	0.0585	1.5040	0.6269	0.1256	0.1568	0.7527
Extra View 01	0.3111	0.0577	1.4936	0.6240	0.1391	0.1672	0.7505
Extra View 02	0.3316	0.0570	1.4825	0.6209	0.1525	0.1776	0.7481
Extra View 03	0.2880	0.0686	1.5040	0.6137	0.1228	0.1590	0.7635
Extra View 04	0.3294	0.0686	1.4825	0.6078	0.1494	0.1803	0.7588
Extra View 05	0.2854	0.0786	1.5040	0.6003	0.1200	0.1611	0.7741
Extra View 06	0.3063	0.0793	1.4936	0.5975	0.1331	0.1720	0.7718
Extra View 07	0.3268	0.0800	1.4825	0.5945	0.1462	0.1829	0.7693

Table 7. **Exact Camera Poses for the Extrapolated Views.** Positions are given in the world frame (MuJoCo’s default metric units, i.e., meters), and orientations are MuJoCo quaternions (q_w, q_x, q_y, q_z) .

Know Your Camera. We adapt Know Your Camera (KYC) from official open-source implementation⁴ to our setting. This method explicitly conditions the policy on camera extrinsic parameters by generating per-pixel 6-dimensional Plücker ray from the camera parameters. We concatenate the Plücker rays into the channel of the original image as suggested in the paper to apply the method to the diffusion policy.

¹<https://github.com/kylesargent/ZeroNVS>

²<https://github.com/sean1295/CLASS>

³<https://github.com/Trevor-emt/Reviwo>

⁴<https://github.com/ripl/CamPoseOpensource>

Table 8. **ZeroNVS Hyperparameters.** Configuration for ZeroNVS for real-world data augmentation.

Hyperparameter	Value
Noise Scheduler	DDIM
Inference Steps	50
Guidance Scale	7.5
FOV deg	13.0°
Default Elevation	-10.0°
Default Azimuth	0.0°
Default Distance	1.0m
Translation Azimuth	{-5.0, 0.0, 5.0}°
Translation Vertical	{-5.0, 0.0, 5.0}cm
Translation Optical	{-5.0, 0.0, 5.0}cm

Table 9. **VILA Training Hyperparameters.** We use a two-stage training pipeline: Stage 1 latent action pre-training and Stage 2 latent behavior cloning.

Hyperparameter	Value
Stage 1: Latent Action Pre-training	
Optimizer	AdamW
Learning Rate	1×10^{-4}
Latent Dimension (D_z)	128
Prediction Horizon (K)	1 ~ 10
Time Indices per Batch (N)	16
Views per Batch (V)	8
Image Resolution	64 × 64
Distance Type	L_2
InfoNCE Temperature (τ)	1.0
λ_1 (\mathcal{L}_{w-NCE})	1.0
λ_2 (\mathcal{L}_{struc})	1.0
Weighting Temperature (β)	0.001
Epochs	100
Gradient Clipping Norm	1.0
Target EMA Coef.	0.001
Target Update Interval (Epochs)	1
IDM Head Hidden Dim.	1024
FDM Head Hidden Dim.	1024
Stage 2: Latent Behavior Cloning	
Optimizer	AdamW
Learning Rate	5×10^{-5}
BC Batch Size	256
Prediction Horizon (K)	10
Image Resolution	64 × 64
Epochs	100

A.5. Diffusion Policy Configurations

For simulation experiments, we used the official open-source implementation⁵ of diffusion policy in Robomimic [23]. The main hyperparameters are summarized in Table 10. All methods (ours and baselines) use the same diffusion-policy architecture and training settings.

For real-world experiments, we utilized the official open-

⁵<https://github.com/ARISE-Initiative/robomimic>

source implementation of the diffusion policy in LeRobot⁶. Configurations for this process are in Table 11.

Table 10. **Diffusion Policy Hyperparameters for Simulations.** Configuration for the diffusion policy used for policy training in simulations.

Hyperparameter	Value
Learning Rate	1×10^{-4}
Encoder Learning Rate (In Fine-tune Setting)	1×10^{-5}
Optimizer	AdamW
Optimizer Scheduler	Cosine
Training Epochs (In Fine-tune setting)	50
Training Epochs (In Frozen setting)	100
Steps per Epoch	1,000
Warmup Steps	500
Batch Size (for Lift)	100
Batch Size (for others)	1,000
Image Resolution	64 × 64
Observation Horizon	1
Prediction Horizon	16
Action Horizon	8
Noise Scheduler	DDIM
Beta Scheduler	squaredcos_cap.v2
Diffusion Training Steps	100
Diffusion Inference Steps	10

Table 11. **Diffusion Policy Hyperparameters for Real-World.** Configuration for the Diffusion Policy for policy finetuning in real-world experiments.

Hyperparameter	Value
Learning Rate	1×10^{-4}
Encoder Learning Rate	1×10^{-5}
Optimizer	AdamW
Optimizer Scheduler	Cosine
Training Steps	200,000
Warmup Steps	500
Batch Size	64
Image Resolution	128 × 128
Observation Horizon	2
Prediction Horizon	16
Action Horizon	16
Noise Scheduler	DDIM
Beta scheduler	squaredcos_cap.v2
Diffusion Training Steps	100
Diffusion Inference Steps	10

B. Additional Experimental Results

B.1. Entropy Results

Tables 12–15 report the same view and action entropy metrics on the remaining tasks (Square, Stack Three, Coffee, and Mug Cleanup). Across all four datasets, we observe the same qualitative trend as in Lift: VILA consistently attains the highest view entropy on both seen and unseen views, while achieving the lowest action entropy among all methods, both before and after policy fine-tuning.

⁶<https://github.com/huggingface/lerobot>

Table 12. **View and Action Entropy (Square).** Entropy-based analysis of representation quality before and after policy fine-tuning in the Square dataset. “Seen” and “Unseen” denote view entropies (higher is better, \uparrow) computed over the 25 views, while “Action” denotes action entropy (lower is better, \downarrow) based on 10 clustered action classes. The upper-bound row corresponds to the entropy of a uniform distribution over 25 views (Seen/Unseen) and 10 action clusters (Action).

Model	Seen (\uparrow)	Unseen (\uparrow)	Action (\downarrow)
Upper Bound	3.219	3.219	2.303
Before Fine-tuning			
VILA (Ours)	2.894	2.705	0.631
CLASS	2.607	1.982	0.861
ReViWo	2.325	1.748	1.316
Fine-Tuned			
VILA (Ours)	2.917	2.712	0.598
Vanilla	2.607	1.982	0.802
CLASS	2.449	1.57	0.912
ReViWo	2.443	1.776	1.384
KYC	1.653	1.143	1.361

Table 13. **View and Action Entropy (Stack Three).** Entropy-based analysis of representation quality before and after policy fine-tuning in the Stack Three dataset. “Seen” and “Unseen” denote view entropies (higher is better, \uparrow) computed over the 25 views, while “Action” denotes action entropy (lower is better, \downarrow) based on 10 clustered action classes. The upper-bound row corresponds to the entropy of a uniform distribution over 25 views (Seen/Unseen) and 10 action clusters (Action).

Model	Seen (\uparrow)	Unseen (\uparrow)	Action (\downarrow)
Upper Bound	3.219	3.219	2.303
Before Fine-tuning			
VILA (Ours)	3.111	3.096	0.362
CLASS	2.950	2.826	0.463
ReViWo	2.592	2.303	1.232
Fine-Tuned			
VILA (Ours)	3.076	3.046	0.339
Vanilla	2.986	2.883	0.488
CLASS	2.886	2.723	0.546
ReViWo	2.667	2.341	1.180
KYC	2.118	2.073	1.053

B.2. UMAP Visualization

Additional view-based UMAPs. In Figures 8–11, we additionally visualize encoder representations across the 25 camera views on Square, Stack-Three, Coffee, and Mug-Cleanup.

Table 14. **View and Action Entropy (Coffee).** Entropy-based analysis of representation quality before and after policy fine-tuning in the Coffee dataset. “Seen” and “Unseen” denote view entropies (higher is better, \uparrow) computed over the 25 views, while “Action” denotes action entropy (lower is better, \downarrow) based on 10 clustered action classes. The upper-bound row corresponds to the entropy of a uniform distribution over 25 views (Seen/Unseen) and 10 action clusters (Action).

Model	Seen (\uparrow)	Unseen (\uparrow)	Action (\downarrow)
Upper Bound	3.219	3.219	2.303
Before Fine-tuning			
VILA (Ours)	2.554	1.924	0.487
CLASS	2.361	1.075	0.700
ReViWo	2.182	1.181	1.053
Fine-Tuned			
VILA (Ours)	2.426	1.632	0.488
Vanilla	2.204	0.809	0.710
CLASS	0.995	0.287	0.812
ReViWo	2.201	1.429	1.222
KYC	1.274	0.457	1.010

Table 15. **View and Action Entropy (Mug Cleanup).** Entropy-based analysis of representation quality before and after policy fine-tuning in the Mug Cleanup dataset. “Seen” and “Unseen” denote view entropies (higher is better, \uparrow) computed over the 25 views, while “Action” denotes action entropy (lower is better, \downarrow) based on 10 clustered action classes. The upper-bound row corresponds to the entropy of a uniform distribution over 25 views (Seen/Unseen) and 10 action clusters (Action).

Model	Seen (\uparrow)	Unseen (\uparrow)	Action (\downarrow)
Upper Bound	3.219	3.219	2.303
Before Fine-tuning			
VILA (Ours)	2.957	2.891	0.452
CLASS	2.564	2.071	0.654
ReViWo	2.383	1.941	1.161
Fine-Tuned			
VILA (Ours)	2.920	2.793	0.404
Vanilla	2.721	2.272	0.614
CLASS	2.153	1.569	0.824
ReViWo	2.437	1.904	1.302
KYC	1.765	1.176	1.142

Action-cluster UMAPs. In Figures 12–16, we reuse the same encoder representations as in the view-based UMAPs, but color them by $K=10$ action clusters obtained by applying k -means to 10-step GT action sequences $\{a_t, \dots, a_{t+9}\}$.

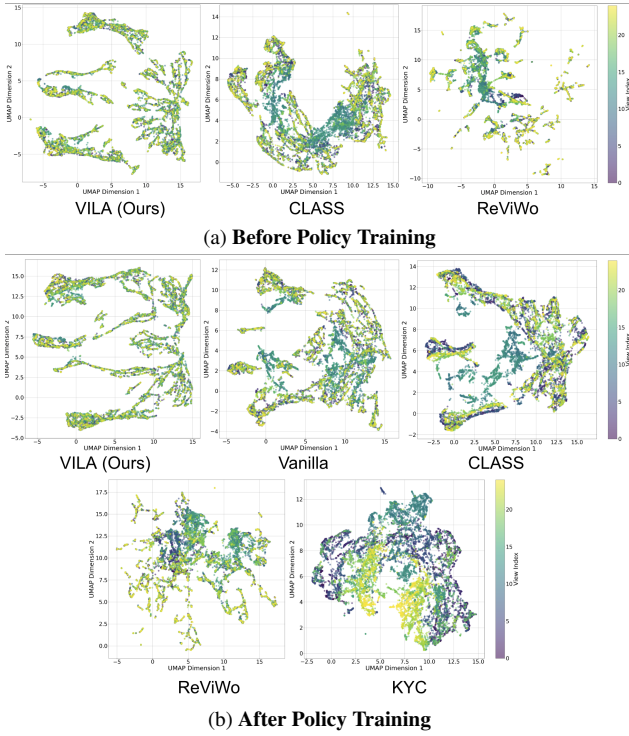


Figure 8. UMAP of encoder representations across 25 views on Square.

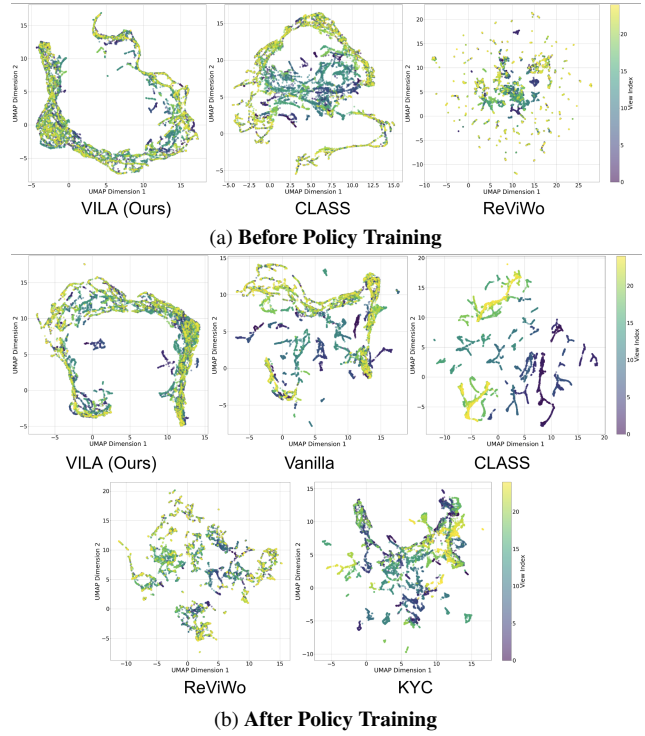


Figure 10. UMAP of encoder representations across 25 views on Coffee.

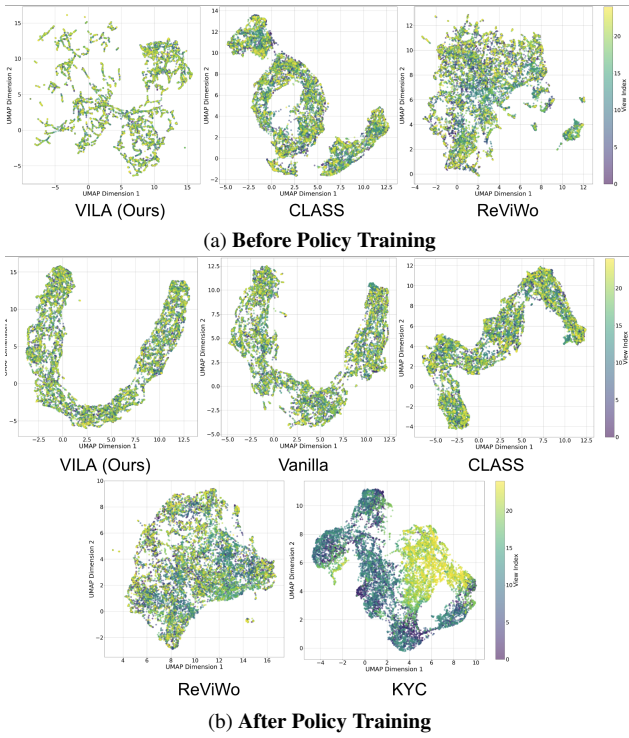


Figure 9. UMAP of encoder representations across 25 views on Stack Three.

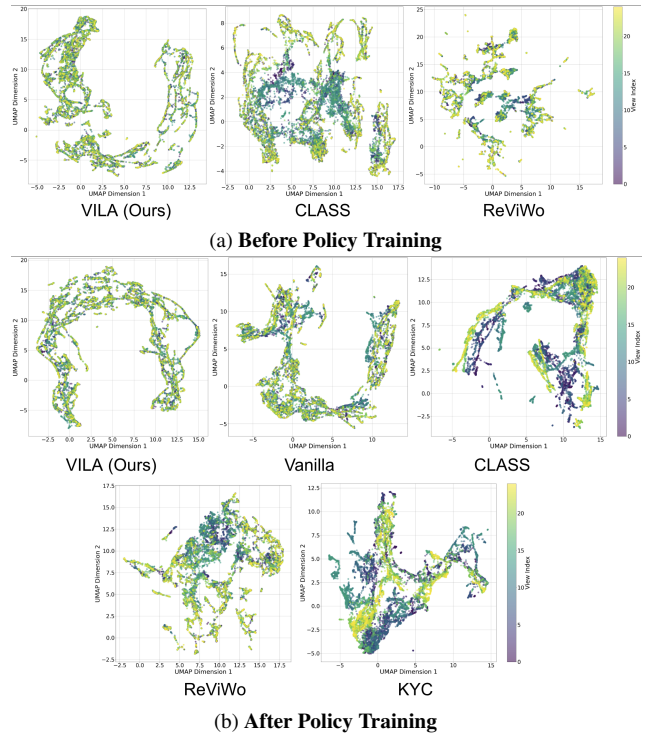


Figure 11. UMAP of encoder representations across 25 views on Mug Cleanup.

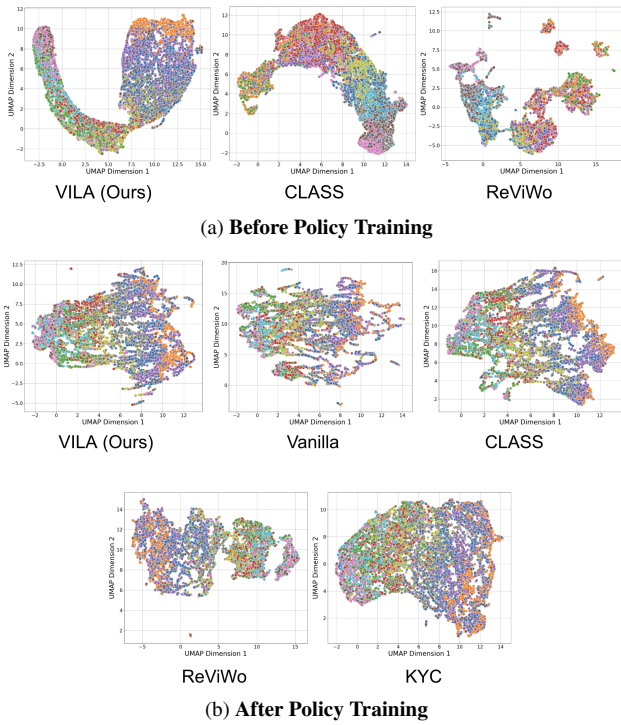


Figure 12. UMAP of encoder representations colored by action clusters on Lift.

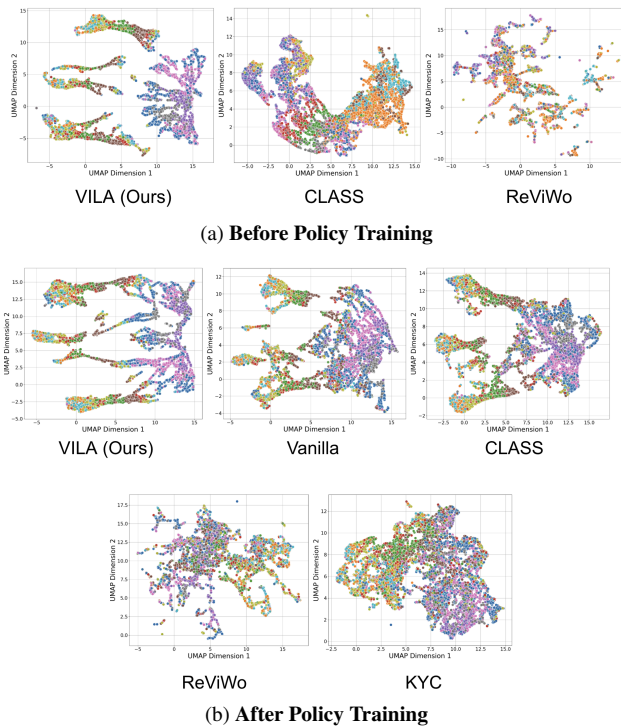


Figure 13. UMAP of encoder representations colored by action clusters on Square.

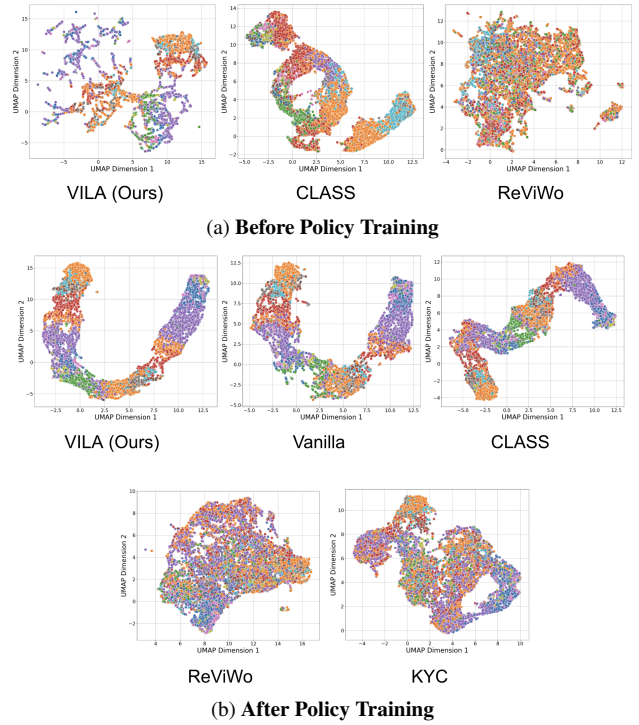


Figure 14. UMAP of encoder representations colored by action clusters on Stack Three.

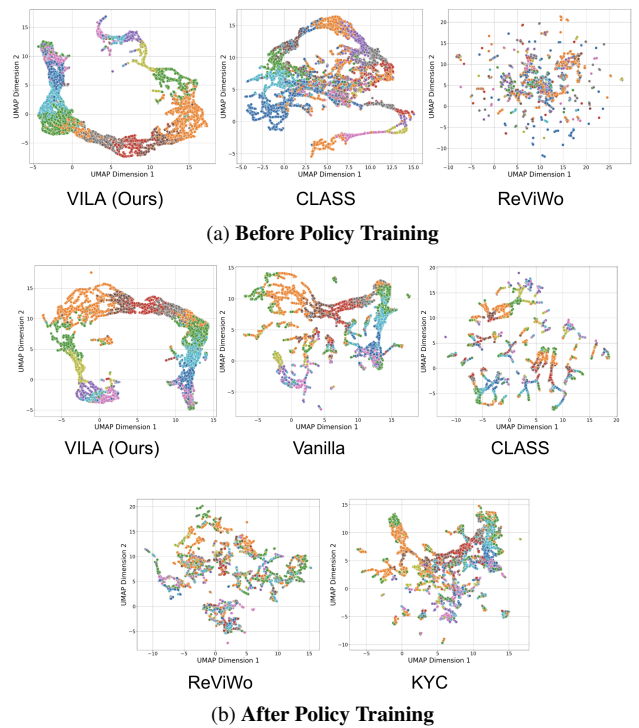


Figure 15. UMAP of encoder representations colored by action clusters on Coffee.

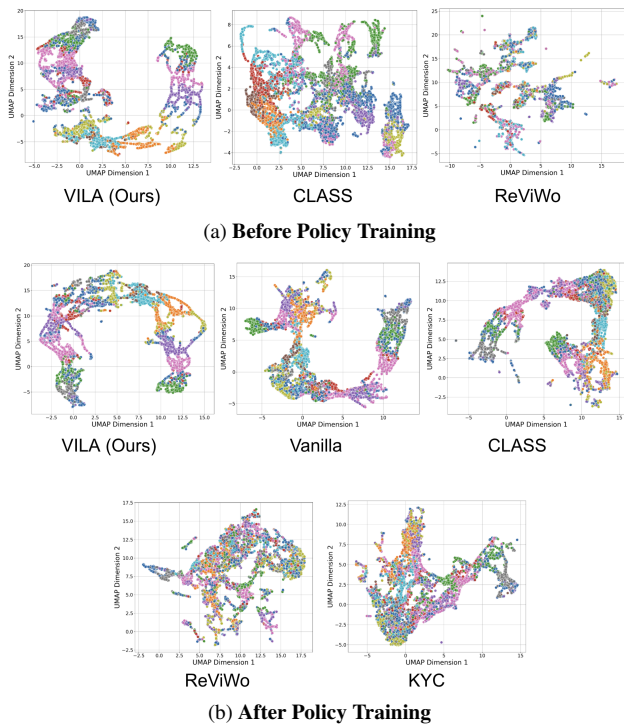


Figure 16. UMAP of encoder representations colored by action clusters on Mug Cleanup.